PERGAMON

Journal of Quantitative Spectroscopy & Radiative Transfer 68 (2001) 75–99

Journal of Quantitative Spectroscopy & Radiative Transfer

www.elsevier.com/locate/jqsrt

Approximations for horizontal photon transport in cloud remote sensing problems

S. Platnick[a,b,*]

[a]*Joint Center for Earth Systems Technology, University of Maryland Baltimore County, Baltimore, MD, USA*
[b]*Code 913, NASA Goddard Space Flight Center, Greenbelt, MD 20771, USA*

Received 2 June 1999

Abstract

The effect of horizontal photon transport within real-world clouds can be of consequence to remote sensing problems based on plane-parallel cloud models. In this paper, analytic approximations for the root-mean-square horizontal displacement of reflected and transmitted photons, relative to the incident cloud-top location, are derived for plane-parallel cloud layers. With anisotropic scattering, separate approximations are needed depending on the order of scattering. When sufficient numbers of photon scatterings occur, an approximation based on random walk theory (photon diffusion) is applicable; when scattering numbers are relatively small, a modification to the diffusion result is used. The resulting formulae are a function of the average number of photon scatterings, as well as particle asymmetry parameter and single scattering albedo. In turn, the average number of scatterings from plane-parallel, vertically inhomogeneous cloud layers can be determined from efficient adding/doubling radiative transfer procedures. The transport approximations are applied to liquid water clouds for typical remote sensing solar spectral bands, involving both conservative and non-conservative scattering. Results compare well with Monte Carlo calculations. Though the emphasis is on horizontal photon transport in terrestrial clouds, the derived approximations are applicable to general anisotropic, multiple scattering, plane-parallel radiative transfer problems. Approximations useful for three-dimensional transport are also given. The complete horizontal transport probability distribution can be described with an analytic distribution specified by the root-mean-square and average radial displacement values. However, it is shown empirically that the average displacement can be reasonably inferred from the root-mean-square value. An estimate for the horizontal transport distribution can then be made from the root-mean-square photon displacement alone.

* Correspondence address: Code 913, NASA Goddard Space Flight Center, Greenbelt, MD 20771, USA.
E-mail address: platnick@climate.gsfc.nasa.gov (S. Platnick).

0022-4073/00/$ - see front matter
PII: S0022-4073(00)00016-9

1. Introduction

Retrieval of cloud properties from multi-channel solar reflectance measurements presume the existence of vertically homogeneous, plane-parallel clouds. However, horizontal variability over many scales is readily observed in liquid water content in situ measurements [1,2], satellite reflectance imagery [3], and ground-based measurements [3,4]. In the vertical, cloud droplet sizes are generally expected to increase with height in non-precipitating clouds. Such size profiles are commonly observed with in situ aircraft [5,6]. Further, deviations from plane-parallel theory as a function of solar and viewing geometry have been observed in visible satellite reflectances [7].

A brute-force determination of cloud inhomogeneity effects on radiation fields, in both the horizontal and vertical, could be found by calculating reflected and transmitted intensities in various spectral bands on a case-by-case basis. However, the spatial measurements needed for such calculations are difficult to obtain in even the most extensive of field campaigns, and certainly not available for large-scale studies. For this reason, simple analytic models have been used to produce horizontal variability for studies of heterogeneous layered cloud systems [8,9]. Regardless of how horizontal structure is realized, it is not obvious how forward calculations from specific case studies or models may be extrapolated for use in global remote sensing inversion algorithms. In such general studies, variability of cloud type and morphology, both temporally and spatially, would have important consequences on the applicability of any case-specific heterogeneity assumptions. Aside from such issues, accounting for realistic inhomogeneities with two and three dimensional radiative transfer codes (e.g., Monte Carlo) is a computationally intensive endeavor.

A simpler and more rudimentary approach is to investigate the spatial scales over which measured reflectances are effectively averaged. Such scales can be determined with relative computational ease for vertically inhomogeneous, plane-parallel cloud layers. The effect of these scales on cloud retrievals can then be inferred as a basic first-step approach towards understanding the practical implications of the plane-parallel assumption (i.e., the horizontal extent over which homogeneity is required for agreement with theory) and the general problem of cloud heterogeneity. This is the approach adopted in this study. In other words, before considering the more difficult question of whether a particular real-world cloud may be effectively plane-parallel for remote sensing purposes, it is useful (and easier) to develop a simple theory for determining the radiative meaning of a plane-parallel geometry. Certainly, plane-parallel *does not* mean that homogeneity is required at distances arbitrarily far from photon incidence. It is convenient to consider the horizontal and vertical scales separately.

For horizontal transport, the displacement of reflected and transmitted photons in a plane-parallel, inhomogeneous, anisotropic scattering medium can be estimated from the average number of scatterings encountered by such photons. The average number of scatterings can, in turn, be determined from an efficient superposition technique developed in previous studies [10,11]. This estimated horizontal displacement can then be used to assess the scales over which horizontal inhomogeneities are important in remote sensing problems. An introductory discussion of vertical transport in visible and near-infrared remote sensing bands is also presented in the above references. Though the transport approximations developed in this paper were motivated by cloud remote sensing issues, they are useful for general anisotropic, multiple scattering problems.

Analytic approximations for the root-mean-square (r.m.s.) horizontal transport of reflected and transmitted photons, applicable to both conservative and absorbing cloud problems, are derived in

Section 2 as a function of the average number of photon scatterings. Results are shown for a variety of solar and viewing geometries, spectral bands, and cloud models. Monte Carlo calculations are used to assess the accuracy of the approximations. A two-parameter gamma function (expressed in terms of the horizontal radial-averaged and r.m.s. displacements) provides a robust analytic form for the horizontal displacement distribution function. In Section 3, it is shown that this average displacement parameter is related to the r.m.s. displacement by a relatively constant factor. Calculations of this factor over a range of cloud thicknesses and angles are presented. These results, along with knowledge of the r.m.s. displacement from Section 2, can then be used to reasonably approximate the full horizontal displacement distribution function.

2. Root-mean-square horizontal transport

In this section, we derive an analytic approximation for the horizontal transport of reflected and transmitted photons within a cloud as a function of the average number of photon scatterings. If average scattering numbers are obtained with relatively time-intensive Monte Carlo calculations, then horizontal transport can, of course, be found directly. Therefore, the development of this transport approximation is of practical use only if more efficient methods are available for determining the average number of scatterings. A means of calculating these averages for plane-parallel, vertically inhomogeneous clouds is available through superposition principles as demonstrated in a companion paper [11]. The derived superposition formulae have been implemented for both reflectance and transmittance problems using fast and efficient adding/doubling numerical routines, and successfully tested against Monte Carlo calculations for various cloud optical thicknesses, viewing geometries, and solar spectral bands (both conservative and non-conservative scattering).

2.1. Transport in an unbounded cloud

We begin with isotropic photon scattering in an unbounded, infinite medium. For a three-dimensional (3-D) random walk, the root-mean-square displacement of photons relative to the starting location after some number of scatterings, n_s^*, is described by the square root of $\langle \tau_r^2 \rangle^* = n_s^* \langle l^2 \rangle$, where the asterisk refers to the isotropic problem, τ_r is the 3-D optical path displacement (product of geometric path and optical extinction), and l is the photon optical path length between scatterings. By definition, the optical path length probability distribution between scatterings is e^{-l}, giving a mean free optical path of unity and $\langle l^2 \rangle = 2$, or $\langle \tau_r^2 \rangle^* = 2n_s^*$. Several approaches to approximating the anisotropic equivalent are possible. We start with an optical path scaling derivation.

Various combinations of cloud optical parameters can give very nearly the same radiative properties when multiple scattering is present. This provides a means of scaling between isotropic and anisotropic scattering problems [12]. Consider a cloud with parameters τ_c, g, and ϖ_0 (cloud optical thickness, droplet asymmetry parameter and single scattering albedo, respectively). Such a cloud will have radiative properties nearly equivalent to one with isotropic scattering (i.e., $g^* = 0$) and $\tau_c^* = \tau_c(1 - \varpi_0 g)$, $\varpi_0^* = \varpi_0(1 - g)(1 - \varpi_0 g)^{-1}$. We wish to determine an appropriate means of scaling the isotropic random walk formulation given above to an anisotropic problem. The optical

displacement for anisotropic scattering can be approximated by scaling the displacement for the complementary isotropic cloud, i.e., $\langle \tau_r^2 \rangle^* \approx \langle \tau_r^2 \rangle (1 - \varpi_0 g)^2$, where the absence of an asterisk on the averaging bracket refers to the anisotropic scattering cloud. The mean free optical path, and likewise $\langle l^2 \rangle$, is unchanged in both problems.

However, a scaling is required for n_s^*. For instance, fewer scatterings are required for reflected photons with isotropic scattering since the incident photon directions are more readily reversed. Similarly, transmitted photons experience fewer scatterings since the isotropic cloud's scaled optical thickness is significantly less than for the anisotropic cloud. Since n_s determines the total mean photon path, it seems reasonable to use an optical path scaling, i.e.,

$$n_s^* \approx n_s(1 - \varpi_0 g). \tag{1}$$

With conservative scattering and $g = 0.85$, n_s would be expected to be a factor of seven greater than for the isotropic problem. The factor would increase with asymmetry parameter and decrease with absorption. This scattering number scaling was also mentioned by Marshak et al. [9] and discussed by Davis and Marshak [13] for conservative scattering. With Eq. (1) and the horizontal optical path scaling, the isotropic expression $\langle \tau_r^2 \rangle^* = 2n_s^*$ becomes $\langle \tau_r^2 \rangle \approx 2n_s(1 - \varpi_0 g)^{-1}$, giving the r.m.s. transport after n_s scatterings as $\tau_{r,r.m.s.} \approx \sqrt{2n_s(1 - \varpi_0 g)^{-1}}$. The wavelength dependence of all variables is implicit.

An alternative, and more insightful derivation, is to consider the average number of scatterings required for photons to *reverse* direction. It can be shown that for a one-dimensional (i.e., 2-stream) analog, this average, $n_{s,rev}$, is given by $\sum_{n=1}^{\infty} n p_B p_F^{n-1} / \sum_{n=1}^{\infty} p_B p_F^{n-1}$, where p_B and p_F are the probability of backwards and forwards scattering, respectively. Allowing for absorption, $p_B + p_F + (1 - \varpi_0) = 1$. Terms in the denominator give the probability for a reversal in direction occurring during the nth scattering; the sum is therefore equal to ϖ_0. The ratio converges to simply $(1 - p_F)^{-1}$. With the 2-stream approximation [14] being consistent with $p_F = \varpi_0(1 + g)/2$, the average number of photon scatterings becomes $2(1 + a - \varpi_0 g)^{-1}$, where $a = 1 - \varpi_0$ is the fractional absorption at each scattering (or co-albedo). Note that for isotropic conservative scattering, the average is 2 as required, and increases with g. Therefore, anisotropic scattering requires a factor

$$x = \frac{n_{s,rev}}{n_{s,rev}^*} = \frac{(1 + a)}{(1 + a - \varpi_0 g)} \tag{2}$$

greater number of photon scatterings for a reversal of direction than for isotropic scattering. Scattering numbers much greater than x ensure randomness for the anisotropic problem and applicability of diffusion approximations. Other than the relatively small absorption term a, this is identical to x from Eq. (1). Monte Carlo calculations show that in 3-D, the average number of scatterings required for a photon to be re-directed into the opposite hemisphere is very close to this 1-D average. With the above interpretation, the mean free isotropic optical path can now be scaled by this same factor x, i.e., $l \to xl$ and $\langle l^2 \rangle \to x^2 \langle l^2 \rangle = 2x^2$. The r.m.s. transport after n_s scatterings is then $\tau_{r,r.m.s.} \approx \sqrt{2xn_s}$. For conservative scattering, this is identical to the result derived from optical path scaling arguments. Even with droplet absorption, the two transport equations are nearly equivalent (the optical path scaling approximation is larger, but typically within 10% for the range of droplet absorption considered in this study, see Table 1).

The accuracy of these unbounded transport approximations needs to be determined before modification to a form suitable for transport in a finite medium. Calculations of $\tau_{r,r.m.s.}$ in

Table 1
Scattering parameters and integrated extinction averaged over typical cloud remote sensing instrument spectral channels, for liquid water droplet size spectra given by a gamma distribution with various effective radii and an effective variance of 0.10. Extinction for a droplet number concentration $N_d = 100\ cm^{-3}$ is given as well as the corresponding geometric distance for unity optical path (for some other droplet concentration, the extinction column should be multiplied by the factor $N_d/100$ and the distance by $100/N_d$).

Effective radius	Spectral band	Single scattering albedo	Asymmetry parameter	Extinction efficiency	Extinction for $N_d = 100\ cm^{-3}$	Geometric distance for $\tau = 1$, $N_d = 100\ cm^{-3}$
(μm)	(μm)	ϖ_0	g	Q_e	(m^{-1})	(m)
5	0.66	1.000	0.843	2.16	0.0122	82
	1.6	0.997	0.796	2.32	0.0131	76
	2.2	0.991	0.782	2.42	0.0137	73
	3.7	0.957	0.762	2.86	0.0162	62
10	0.66	1.000	0.861	2.10	0.0475	21
	1.6	0.994	0.843	2.19	0.0495	20
	2.2	0.979	0.834	2.25	0.0509	20
	3.7	0.900	0.794	2.33	0.0527	19
15	0.66	1.000	0.869	2.08	0.1056	9.5
	1.6	0.991	0.859	2.14	0.1090	9.2
	2.2	0.969	0.860	2.18	0.1108	9.0
	3.7	0.864	0.843	2.27	0.1154	8.7

a homogeneous unbounded medium were tested with Monte Carlo calculations by specifying g, ϖ_0 and a fixed number of photon scatterings, n_s. These results were then compared with the above expressions. For a large number of scatterings (i.e., where n_s/x is large, or more specifically $n_s > 20$, $n_s^* > 3$), $\tau_{r,r.m.s.}$ is indeed proportional to $\sqrt{n_s}$ and accurately described by diffusive transport. However, for small scattering numbers ($n_s < x$), path direction is clearly not random for the anisotropic problem and transport should be of the form $\tau_{r,r.m.s.} \propto n_s^y$, where $y > 1/2$. For instance, in the extreme situation where $g = 1.0$ ($x \to \infty$ for conservative scattering) there is no deviation in photon direction regardless of scattering number, and the r.m.s. optical path is simply the product of n_s and the r.m.s. optical displacement per scattering, i.e., $y = 1$ and $\tau_{r,r.m.s.} = \sqrt{2}n_s$. Calculations show that with typical values of g for cloud droplets (see Table 1), y increases from 0.75 to 0.80 as g increases from 0.75 to 0.85, respectively, for the small scattering number regime. An excellent fit over the broad range $g = 0.65$–0.90 was found to be $y = 0.85 p_F$. Combining transport formulae for both scattering number regimes gives the approximate transport for any scattering number. In summary, for unbounded 3-D transport with anisotropic scattering, we have

$$\tau_{r,r.m.s.} \approx \sqrt{2xn_s}, \quad n_s > x, \tag{3a}$$

$$\tau_{r,r.m.s.} \approx \sqrt{2}n_s^y \approx \sqrt{2}n_s^{0.85 p_F}, \quad n_s < x, \tag{3b}$$

where the approximation for y is appropriate for cloud droplets in the remote sensing bands of interest.

Monte Carlo calculations of 3-D transport as a function of n_s were compared with Eq. (3) over a range of cloud droplet g and ϖ_0 (Table 1). The boundary between the two regimes was chosen as the intersection of the two curves, which occurs at $n_s = x^{(2y-1)^{-1}}$. As a check, note that if $g = 0$, then $x = 1$ and the boundary is at $n_s = 1$, meaning the diffusion approximation is appropriate for all orders of scattering as it should be with isotropic scattering. Example are shown in Fig. 1 for both

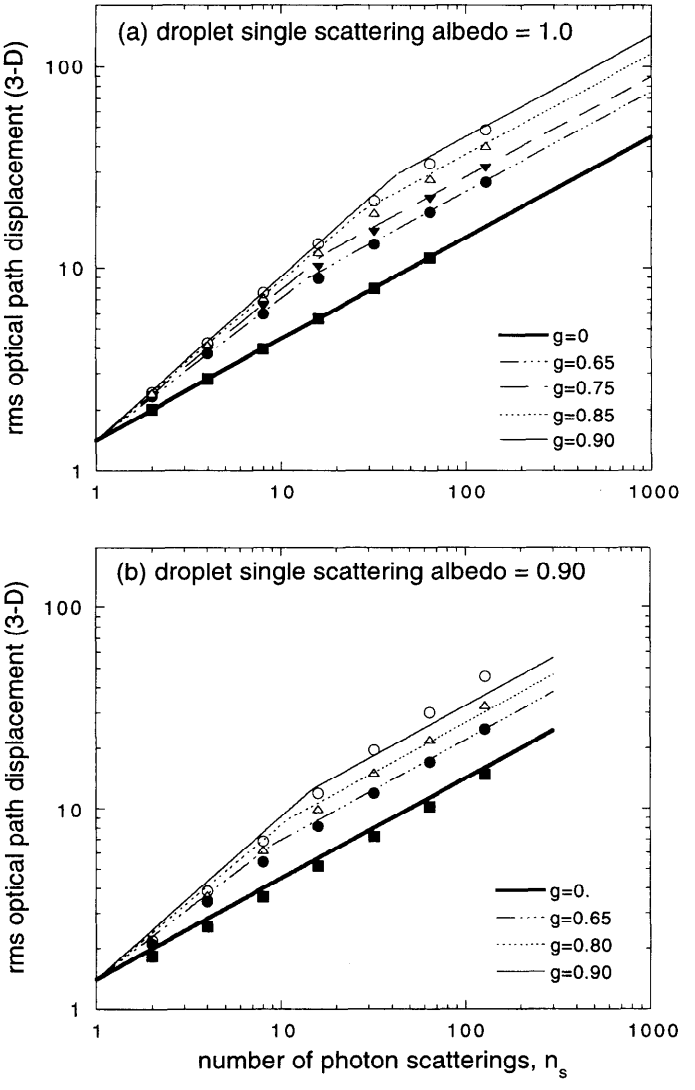

Fig. 1. Monte Carlo calculations (symbols) of the root-mean-square (r.m.s.) optical path displacement in three dimensions, $\tau_{r.m.s.}$, after n_s scatterings, compared with approximations given by Eqs. (3a) and (3b) (lines). Results are shown as a function of asymmetry parameter for (a) conservative scattering, and (b) scattering with large absorption (e.g., the 3.7 μm spectral band in Table 1).

conservative scattering and $\varpi_0 = 0.90$ (e.g., 3.7 μm spectral band). Excellent agreement for both regimes is seen. The approximation error is of course greatest near the regime boundaries, but still within about 5%. A slight increase in the diffusion regime slope for the highly absorbing case at $g = 0.9$ is evident. However, average scattering numbers appropriate to cloud problems in this band are practically limited to the small scattering number regime [11].

2.2. Transport in a finite cloud

We now consider horizontal transport. The problem of interest is that of a finite layered cloud with incidence from above, and a specified optical thickness. If transport in each dimension is uncorrelated, the individual mean-square displacements are equivalent and the two-dimensional optical path displacement (e.g., the horizontal plane for the cloud problem) is then $\langle \tau_H^2 \rangle = 2/3 \langle \tau_r^2 \rangle$, where the subscript H refers to horizontal transport. This expression requires a large number of scatterings for the anisotropic cloud because of the need for sufficient directional randomness. Further, it is only strictly valid for unbounded transport with a specified number of scatterings. Substitution of the 3-D diffusion transport derivation gives $\langle \tau_H^2 \rangle \approx 4/3 x n_s$.

For a finite cloud, reflected and transmitted photons are described by a distribution of n_s. The simplest way of accounting for bounded transport, is to replace n_s with the average number of scatterings, $N_s \equiv \langle n_s \rangle$, giving $\tau_{r,r.m.s.} \approx 2\sqrt{xN_s/3}$ in the diffusion domain. As mentioned, the average number of photons scatterings in a plane-parallel, vertically inhomogeneous cloud can be determined from superposition calculations. Use of N_s was found to provide an excellent approximation to horizontal transport for both reflected and transmitted photons in the large average scattering number regime (synonymous with large cloud optical thickness if absorption is relatively weak [11]). In a similar fashion, a random walk derivation for geometric horizontal transport in terms of cloud geometric thickness was pursued by Davis et al. [15] for conservative scattering in discussing the characteristic physical spot size of light scattered from a narrow beam. Our diffusion domain result is similar to their formulation if the average number of scatterings is replaced by a functional dependence on cloud thickness (e.g., from asymptotic theory applied to flux reflectance or transmittance).

When N_s/x is small (i.e., small optical thickness or large absorption), photon scatterings are insufficient for transport in each dimension to be uncorrelated, and horizontal transport within the cloud is largely governed by the geometry of the situation. In the extreme case where only one scattering occurs before reflection or transmission, the photon's horizontal exit displacement would be proportional to the sum of the sine of the solar and viewing angles, $\sqrt{(1-\mu_0^2)}$ and $\sqrt{(1-\mu^2)}$, respectively (ignoring azimuthal changes in direction). The standard notation μ_0 and μ has been used for the cosine of the solar and viewing angles, respectively. It is worth considering the suitability of a simple average of the two horizontal projections, i.e., $\langle 1-\mu^2 \rangle \equiv \frac{1}{2}[(1-\mu^2)+(1-\mu_0^2)]$, for approximating the geometric dependence relevant for small numbers of scatterings. Transport then takes the form of $\tau_{r,r.m.s.} \propto \sqrt{2\langle 1-\mu^2 \rangle} n_s^y$. Changes in azimuth direction will clearly modify the overall horizontal translation. Arbitrary constants are common in diffusion and asymptotic approximations [12] and the present situation is no exception. In this case, calculations indicate that an additional factor of about $\sqrt{3/2}$ is needed to properly account for the geometric effect in the spectral bands of interest. Modifications to Eqs. (3a)

and (3b) therefore give

$$\tau_{\mathrm{H,r.m.s.}} \approx \frac{2}{\sqrt{3}}\sqrt{xN_{\mathrm{s}}}, \quad N_{\mathrm{s}} > x, \tag{4a}$$

$$\tau_{\mathrm{H,r.m.s.}} \approx \sqrt{3\langle 1-\mu^2\rangle}N_{\mathrm{s}}^{0.85p_{\mathrm{F}}}, \quad N_{\mathrm{s}} < x. \tag{4b}$$

Again, the wavelength dependence of all optical variables is understood. In addition, N_{s} is a strong function of cloud optical thickness and solar/viewing geometry. Note that Eq. (4) approximates both reflected and transmitted transport, the difference between the two cases being governed solely by the average number of scatterings.

There are several approaches to delineating between the two regimes of Eq. (4). First, as used with the unbounded transport derivation, the number of scatterings separating the two regimes, call it N'_{s}, can be defined by the intersection of the two curves, i.e.,

$$N'_{\mathrm{s}} = \left[\frac{2}{3}\sqrt{\frac{x}{\langle 1-\mu^2\rangle}}\right]^{1/(y-1/2)}. \tag{5}$$

This gives excellent agreement across all range of scattering numbers for nominal geometries (e.g., Fig. 2 where $\mu_0 = 0.65$, $\mu = 0.85$). However, an obvious problem will occur for near-normal directions when $\langle 1-\mu^2\rangle \approx 0$. Then N'_{s} becomes so large that only the small scattering number regime approximation (Eq. (4b)) applies. For example, in the visible if $\mu_0 = 0.95$, $\mu = 0.85$, then $N'_{\mathrm{s}} > 130$ (corresponding to a cloud optical thickness of about 30 and 80 for transmittance and reflectance, respectively). Clearly, applicability of Eq. (4a) should ultimately depend on scattering number, not geometry. One way around this difficulty is to set an arbitrary maximum for N'_{s} that is sufficient to guarantee applicability of the diffusion approximation. Calculations indicated a practical upper limit of $N'_{\mathrm{s,max}} = 4x$ for best overall accuracy of Eq. (4), i.e., a factor of four greater than the isotropic equivalent scattering number. However, when N'_{s} is fixed, continuity between Eqs. (4a) and (4b) requires adjustment of the slope of y to

$$y = \frac{1}{2} + \frac{\log\left(\frac{2}{3}\sqrt{\frac{x}{\langle 1-\mu^2\rangle}}\right)}{\log(N'_{\mathrm{s,max}})}. \tag{6}$$

This was the approach adopted in the results that follow. In summary, if application of Eq. (5) for a particular geometry gives $N'_{\mathrm{s}} > N'_{\mathrm{s,max}}$ then N'_{s} is set to $N'_{\mathrm{s,max}}$ and Eq. (6) used to determine the appropriate value of y.

2.3. Horizontal transport examples

Comparisons between Monte Carlo calculations and Eqs. (4)–(6) for reflectance and transmittance, using the average number of scatterings determined from superposition formulae, are shown in Fig. 2 as a function of cloud optical thickness and spectral band (or droplet absorption, see Table 1). Superposition calculations are based on the matrix formulations of Twomey et al. [16,17] which average over finite bin sizes in μ and μ_0. A 20-stream implementation is used, with equal bin sizes of $\mu_i \pm \Delta\mu$, for $\mu_i = 0.05, 0.15, \ldots, 0.95$ and $\Delta\mu = 0.05$, for both view and solar zenith directions. For

consistency, Monte Carlo calculations are averaged over the same bin sizes. Scattering numbers, as well as all other calculations in this paper, are for the azimuthally averaged radiation field only. Though the superposition formulae may be applied to vertically inhomogeneous cloud layers, the present calculations are for a homogeneous cloud with a droplet effective radius r_e, of 10 μm [18] (nominal for non-precipitating liquid water clouds). Both optical path axes have been scaled to an extinction efficiency of 2.0 to avoid the wavelength dependence occurring for the same physical cloud specification (i.e., $l = 2l_\lambda/Q_{e,\lambda}$, where l_λ and $Q_{e,\lambda}$ are the wavelength-dependent optical path and extinction efficiency, respectively, and l is the wavelength-independent quantity plotted). Since the average number of scatterings in plane-parallel cloud layers obey reciprocity [11], Fig. 2 is also valid upon exchange of solar and viewing directions.

As seen in Fig. 2, the approximations of Eqs. (4a) and (4b) for the separate regimes are in excellent agreement with Monte Carlo calculations. Horizontal displacement in this discussion is the r.m.s. *exit* location of reflected and transmitted photons relative to the entry location. This is somewhat overestimated for optically thick clouds. Also of interest is the r.m.s. *maximum* horizontal displacement achieved within the cloud (greater than or equal to the exit displacement). The r.m.s. maximum displacement determined from Monte Carlo calculations (also shown in Fig. 2a) was about 5–13% greater than the exit displacement, as cloud optical thickness increased from 5 to 40, respectively, generally independent of the spectral band. Eq. (4) actually gives better agreement with the maximum displacement for reflectance transport. The relative errors in the plots of Fig. 2 are shown in Fig. 3. The boundary between the two regimes is indicated by the peak in error. Because N_s' corresponds to an optical thickness of about 15 in the visible band for the chosen angles, this is the thickness of the peak error. Overall, there is a slight positive bias to the approximations. The only exception is for transmittance with large absorption (3.7 μm band). Otherwise, relative error is generally between 0 and 5% for optical thickness greater than 4.

Due to the nonlinearity in Eq. (3), it is not obvious that average values of the scattering number or the bulk cloud asymmetry parameter correctly represent the effect of a distribution of values. An example of the scattering number probability distributions for reflectance and transmittance, $p(n_s^r)$ and $p(n_s^t)$, respectively, are shown for flux quantities in Fig. 4a as determined from Monte Carlo calculations (for a visible spectral band, $\tau_c = 10$, $r_e = 10$ μm). These curves are closely related to the path length distribution. In addition, reflected and transmitted photons clearly do not observe the same overall scattering statistics. Reflected photons experience more backward scatterings on average, resulting in an *effective* asymmetry parameter that is less than the overall; likewise transmitted photons experience a larger effective asymmetry parameter. As an example, with $\tau_c = 10$, $g = 0.86$, $\varpi_0 = 1$, the calculated asymmetry parameter determined from Monte Carlo calculations was found to be about 0.84 and 0.88 for reflected and transmitted photons, respectively (i.e., a separate tally was made of the average cosine of the scattering angle for each order of scattering undergone by reflected and transmitted photons). Example plots of $g(n_s)$ for this example are shown in Fig. 4b. The departure of the effective values from g increases as optical thickness decreases and the average number of scatterings is reduced. For the same reason, the departure increases when absorption is present. With $\tau_c = 10$, $g = 0.84$, $\varpi_0 = 0.979$ (2.2 μm spectral band with a 10 μm droplet effective radius), the effective asymmetry parameter is calculated to be 0.81 and 0.87 for reflected and transmitted photons, respectively; for $g = 0.79$, $\varpi_0 = 0.900$ (3.7 μm spectral band), effective values are 0.70 and 0.85, respectively. From Eq. (4), a smaller effective

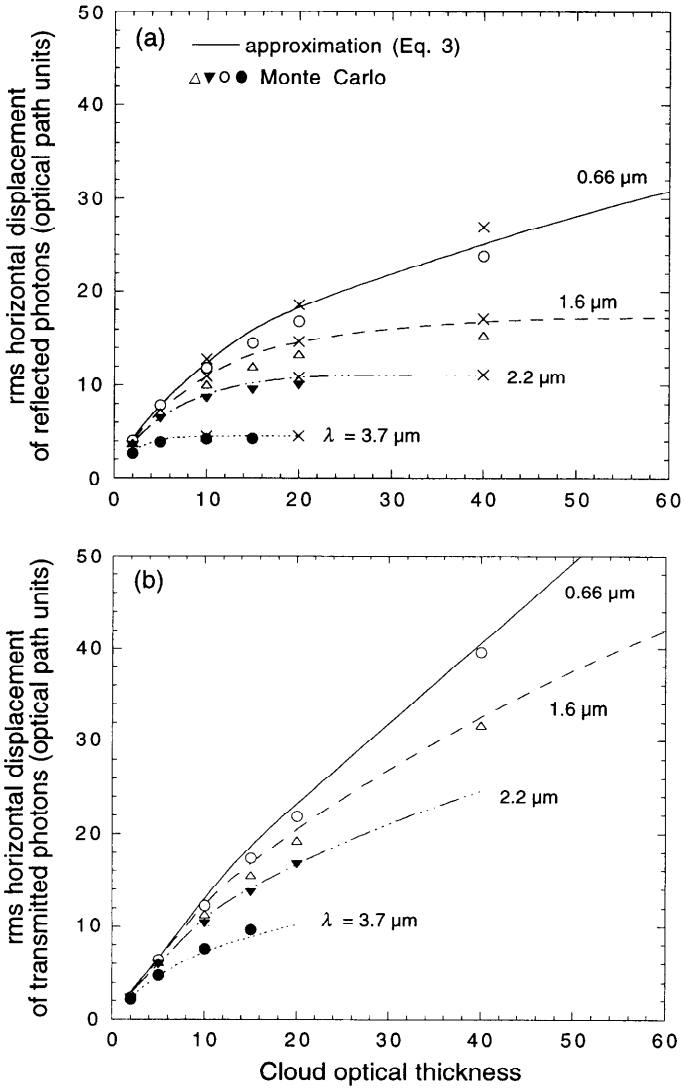

Fig. 2. Root-mean-square horizontal optical path displacement, $\tau_{H,r.m.s.}$, of (a) reflected, and (b) transmitted photons as a function of cloud optical thickness in four spectral bands (from Table 1). Monte Carlo calculations (symbols) are compared with the transport approximation of Eqs. (4a) and (4b) (lines) for a homogeneous cloud with effective radius $r_e = 10$ μm, cosine of solar and viewing angles of $\mu_0 = 0.65$ and $\mu = 0.85$, respectively. Monte Carlo results are for the r.m.s. *exit* displacement except in (a) where ×'s indicate the r.m.s. *maximum* horizontal displacement.

g (corresponding to reflectance) gives rise to less horizontal displacement, and conversely for a larger g (transmittance).

For a small number of scatterings, both the $p(n_s)$ and $g(n_s)$ distributions are relevant (Fig. 4). In principle, improved estimates of horizontal transport in this regime can be made by incorporating

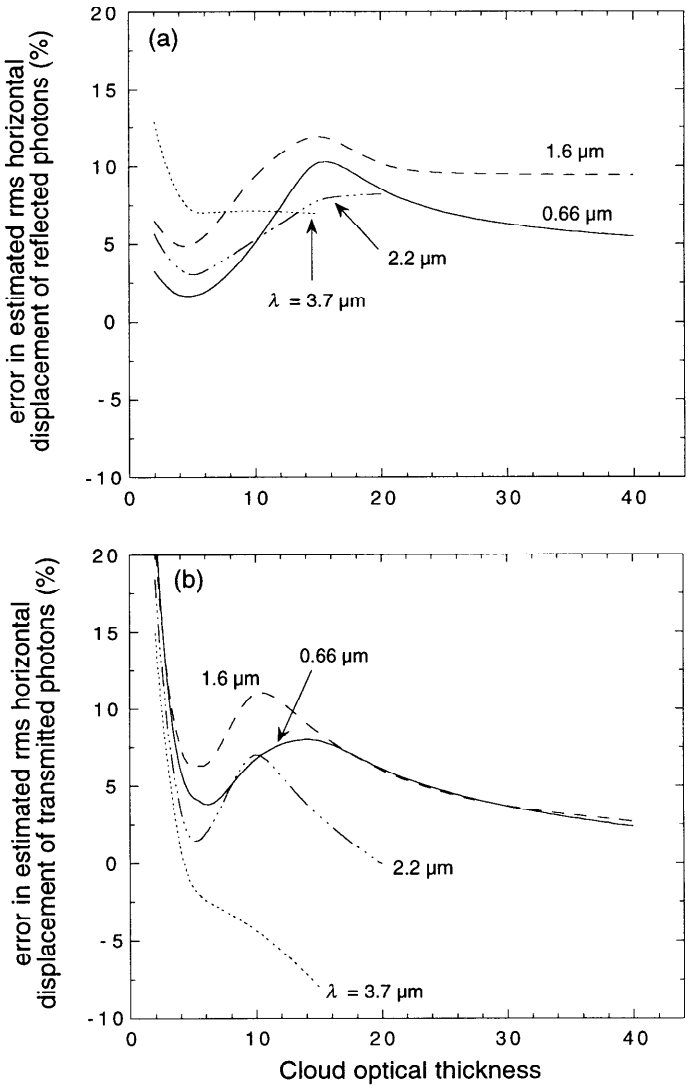

Fig. 3. Relative error (%) in the horizontal transport approximations of Fig. 2 for (a) reflected and (b) transmitted photons.

the distributions into Eq. (4b) giving

$$\tau_{\mathrm{H,r.m.s.}} \approx \int_0^\infty p(n_s)\left[\sqrt{3\langle 1-\mu^2\rangle}\; n_s^{0.85\, p_F(g(n_s))}\right] \mathrm{d}n_s. \tag{7}$$

Eq. (4a) can be modified correspondingly, though for large numbers of scatterings the $p(n_s)$ distribution should dominate. Though these modified equations require Monte Carlo calculations

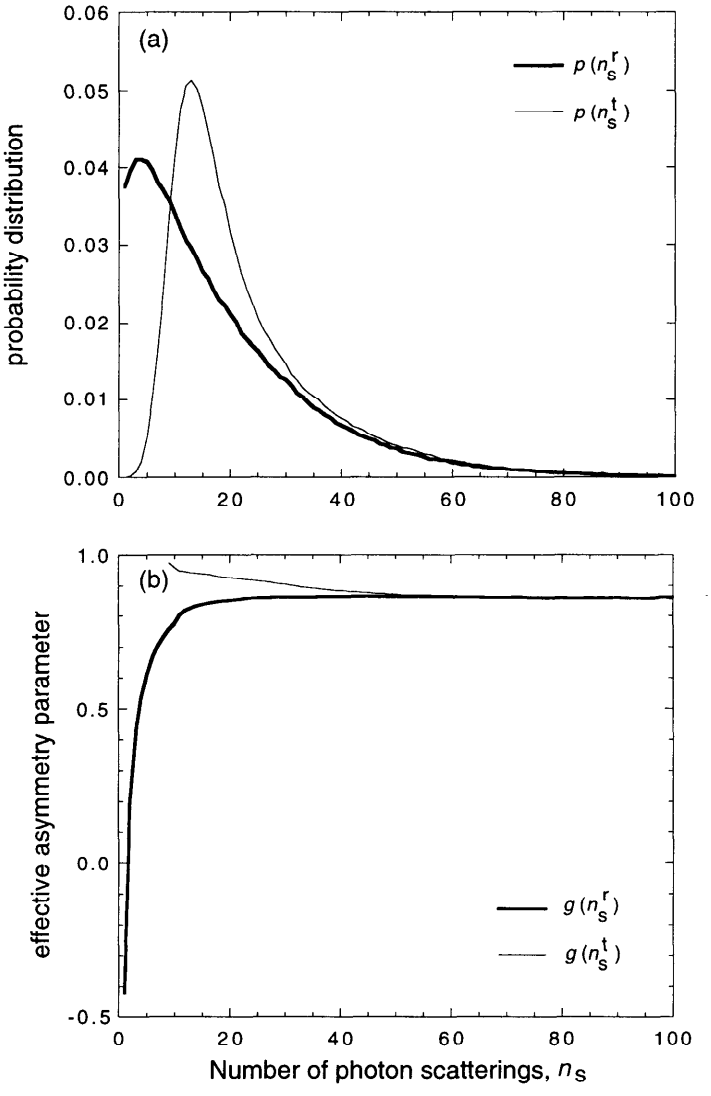

Fig. 4. (a) Probability distribution for the number of scatterings encountered by reflected and transmitted photons, n_s^r and n_s^t, respectively, and (b) effective asymmetry parameter determined from the accumulated scattering angle acquired by all photons with n_s^r and n_s^t scatterings. From Monte Carlo calculations of flux reflectance and transmittance for the visible band of Table 1, for a cloud with optical thickness $\tau_c = 10$, $r_e = 10\ \mu m$, and $\mu_0 = 0.65$.

of the distribution functions, and so cannot be obtained solely from superposition calculations, it is instructive to determine whether they provide better estimates of horizontal transport. Application of Eq. (7) does reduce the error for reflectance transport by about a factor of 5. However, for transmittance, little improvement is made (1–2% absolute reduction in relative error). In the large numbers of scatterings regime, use of the distributions improves the transport approximation over

some limited range of optical thickness, but little is gained overall and Eq. (4a) is equally satisfactory. So, with the exception of reflectance transport at small optical thicknesses, the first moment of the scattering number size distribution and a single bulk asymmetry parameter are as successful in estimating horizontal transport as the complete distributions of Fig. 4.

The angular dependence of transport is shown for a visible band in Figs. 5a and b, where N_s and $\tau_{H,r.m.s.}$ are given as a function of the cosine of the viewing and solar zenith angles for a cloud with optical thickness 10 (only Monte Carlo calculations are shown). For reflected photons, the larger scattering numbers, and hence transport, occur across a relatively broad angular range towards

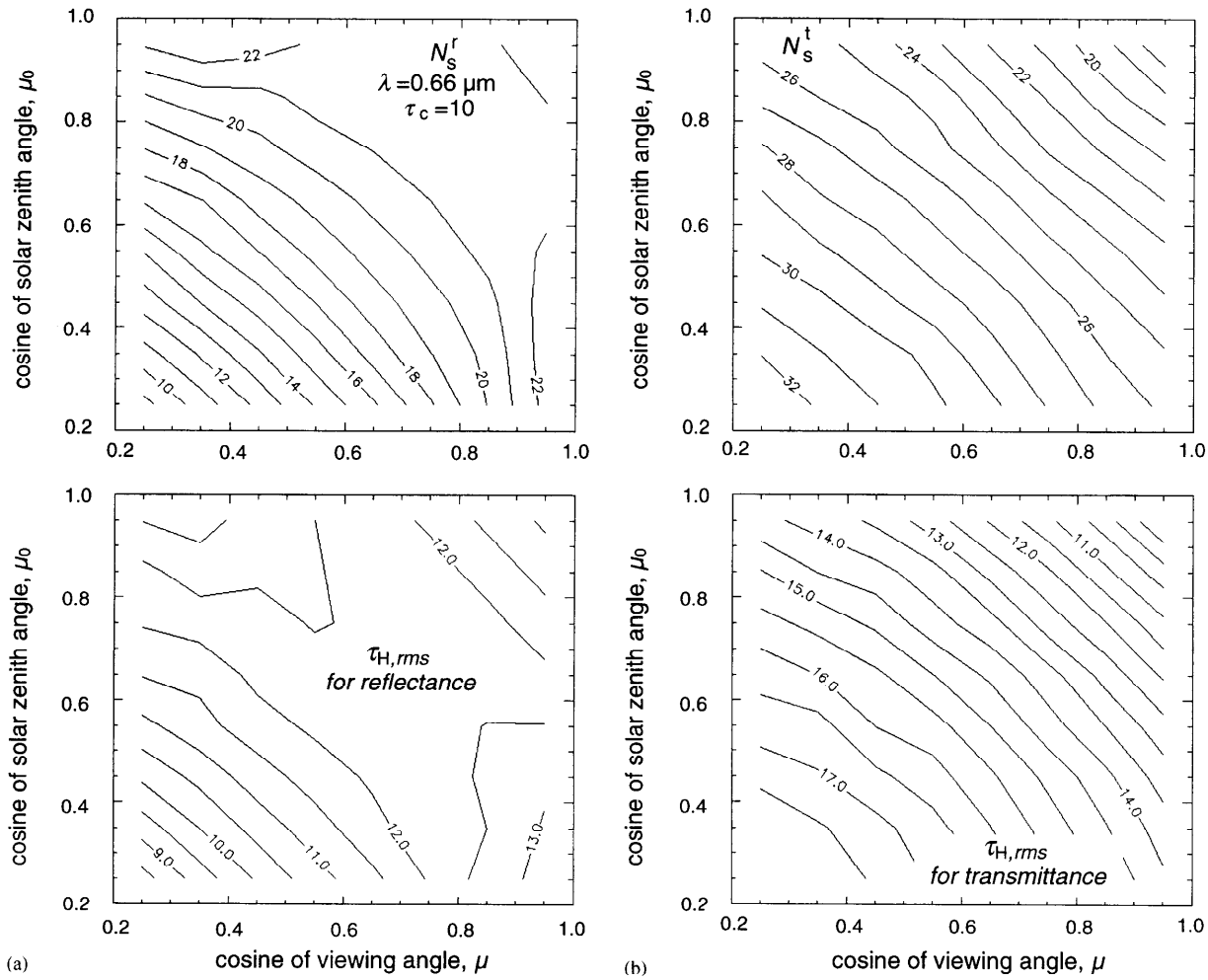

Fig. 5. (a) Monte Carlo calculations of the average number of scatterings, N_s^r, and the r.m.s. horizontal displacement, $\tau_{H,r.m.s.}$, of reflected photons as a function of angles μ_0 and μ for the visible band of Table 1, with $\tau_c = 10$ and $r_e = 10$ μm. Note the reciprocity with angle (exact symmetry is limited by Monte Carlo statistical noise). (b) Same as Fig. 5a but for transmitted photons.

nadir views and zenith solar positions. For the cloud of this example, the azimuthally averaged bidirectional reflectance generally decreases with increasing μ or μ_0. An exception is as the viewing (solar) position moves close to nadir (zenith) and reflectance begins to increase, peaking at a broad maximum corresponding to the rainbow scattering angle. The location of larger scattering numbers in the contour plot of Fig. 5a therefore correspond to smaller bidirectional reflectance values. However, as the cloud becomes thinner (e.g., $\tau_c \approx 2$), both reflectance *and* average scattering number decrease with μ. In this case, scattering numbers are small (~ 5) and larger μ values have the effect of limiting the optical path available for scattering and subsequent reflection. For transmittance (Fig. 5b), the largest scattering numbers are seen to occur for horizon views and solar positions, corresponding to smaller bidirectional transmittance values. Again, for thinner clouds, the opposite may occur. The correspondence between average scattering numbers and the bidirectional quantities as a function of angle therefore depends on optical thickness. In contrast, at any specific set of angles, as long as reflectance continues to increase with optical thickness, then of course so does the average scattering number. Likewise, the monotonic decrease in transmittance with optical thickness is always accompanied by an increase in the average number of scatterings [11]. In both the reflectance and transmittance examples of Fig. 5, horizontal transport is greater than cloud optical thickness, with the ratio $\tau_{\text{H.r.m.s.}}/\tau_c$ ranging from about 1.0–1.2 for reflectance to 1.0–1.7 for transmittance. The ratio decreases with increasing optical thickness (except for conservative transmittance, see Fig. 2).

The geometric, or physical, photon path is of practical interest when considering the scales of horizontal transport implied by plane-parallel theory. However, it is the optical path, used in the previous derivations, that is the more fundamental quantity. For example, two clouds with very different physical thicknesses can have the same optical thickness, and thereby identical optical path transport. The physical and optical paths are related by optical extinction, which is in turn, a function of cloud microphysics. Table 1 gives the Mie scattering parameters for liquid water droplets in the typical conservative and absorbing remote sensing bands of Fig. 2, across a nominal range of effective radii for non-precipitating liquid water clouds. The extinction (m^{-1}) and its inverse is given in the last two columns for a droplet number concentration, N_d, of 100 cm^{-3}. As an example, for a cloud with this droplet concentration and an effective radius of 10 μm, an optical path of unity corresponds to a geometric path of about 20 m. Referring to the cloud of Fig. 2, with $\tau_c = 20$ the horizontal r.m.s. geometric displacement of reflected photons varies from 80 m in the 3.7 μm band to about 350 m in the visible; for transmittance, the displacement varies from about 250–500 m, respectively. Note that for some other droplet concentration, the geometric paths derived from the table must be scaled by $100/N_d$. For example, a somewhat "cleaner" cloud having fewer cloud condensation nuclei and $N_d = 50$ would result in twice the geometric displacement; likewise, a polluted cloud would result in less displacement. The cloud droplet size distribution used in all calculations is a modified gamma distribution [18] with an effective variance of 0.10.

Cloud retrieval algorithms and radiative balance calculations are typically based on plane-parallel cloud models. The r.m.s. horizontal displacement provides a useful scale over which a cloud should be effectively plane-parallel for such an assumption to be valid. Alternatively, these are the scales over which photons must be collected by an imaging instrument such that cloud regions outside of the viewing area contribute little to the measured signal. The r.m.s. displacement is also related to the scale break, or radiative smoothing scale, found in spectral analysis of high resolution imagery [9,15]. More specific statements require knowledge of the complete distribution

for photon transport. This is the subject of Section 3. In the preceding examples, note that the r.m.s. horizontal photon transport through the plane-parallel cloud was greater than the 10's of meter pixel sizes obtained with high spatial resolution satellite and aircraft imagers (e.g., Landsat, ASTER [19], MODIS Airborne Simulator [20]), but on the order of the 250–1000 m resolution obtained by meteorological and global change satellites (AVHRR, MODIS [19]).

2.4. Error calculations

An empirical estimate of the horizontal transport relative error resulting from Eqs. (4)–(6) was obtained by comparison with Monte Carlo calculations across a range of cloud optical thicknesses, solar and view angles, and spectral bands. Calculations of relative error versus viewing and solar angles are shown in Figs. 6a and b for the visible and 2.2 μm bands, respectively, and at three optical thicknesses ($\tau_c = 5,10,20$). As in Fig. 3, the error peaks at the boundary between the two scattering regimes of Eqs. (4a) and (4b). The highly structured contour lines result from the changing position of this boundary, i.e., N_s', with geometry. Exact symmetry in the plots are a result of averaging the Monte Carlo results for reciprocal pairs of angles; the average number of scatterings used in the approximations already obey reciprocity due to the nature of the superposition numerical technique. In addition to improving the Monte Carlo statistical noise, the forced reciprocity in the resulting error calculations generates more easily interpretable contour plots. The angular detail shows some increase in error toward overhead solar and viewing positions at the larger thicknesses, but overall, error is generally within 10%.

3. Approximations for the transport distribution

It was suggested by van de Hulst [12] that a two-parameter gamma distribution provides a standard analytic form for photon path lengths. Marshak et al. [9] showed that such a distribution works well for conservative horizontal photon transport in both plane-parallel and fractal clouds. They subsequently used the distribution to improve optical thickness retrievals in fractal clouds [21]. The distribution was also used for path length retrieval estimates in the visible [22]. For present purposes, an azimuthally symmetric, normalized standard distribution function can be written as

$$p(\tau_H) \approx \frac{\tau_H^{\alpha-1}}{\Gamma(\alpha)\left(\frac{\langle\tau_H\rangle}{\alpha}\right)^{\alpha}} e^{-\alpha\tau_H/\langle\tau_H\rangle}, \tag{8}$$

where τ_H is the horizontal optical path displacement of exiting photons, $\langle\tau_H\rangle$ the average 1-D horizontal displacement, and $\alpha = (f^2 - 1)^{-1}$ with $f = \tau_{H,r.m.s.}/\langle\tau_H\rangle$. The denominator provides the appropriate normalization. The average quantity introduced above should not be confused with the average displacement in the 2-D horizontal plane, which would be zero for overhead incidence (i.e., a mean exit location at the origin with exiting photons distributed in an azimuthally symmetric pattern). Rather, average displacement is defined along the τ_H dimension (i.e., the radial dimension in cylindrical coordinates) giving a non-zero average since negative τ_H locations are not possible. A value of $\alpha = 1, f = \sqrt{2}$ corresponds to an exponential distribution. When $\alpha > 1, f < \sqrt{2}$ the

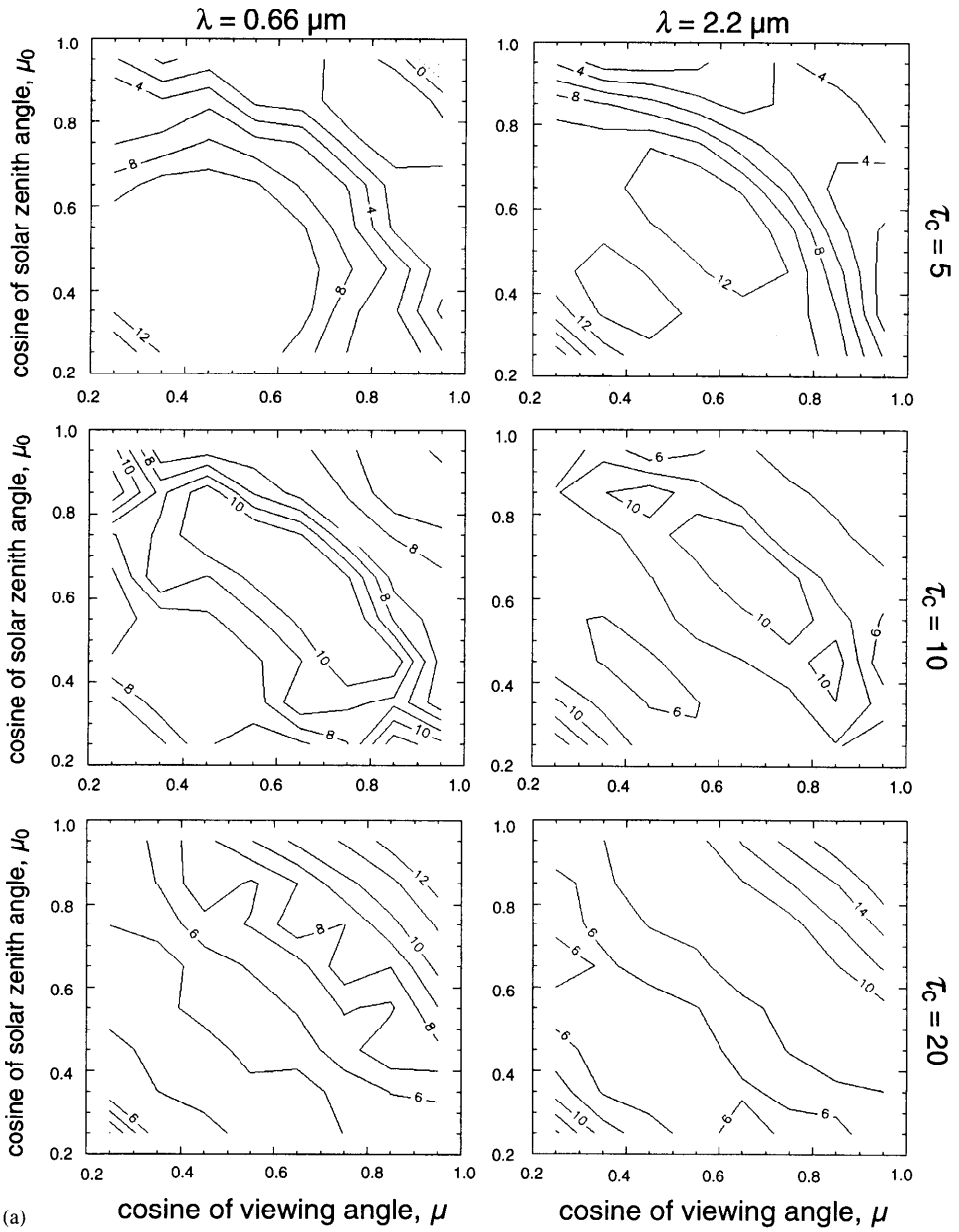

Fig. 6. (a) Relative error (%) in the estimated r.m.s. horizontal displacement of reflected photons using Eqs. (4a) and (4b) (along with either Eq. (5) or (6)) compared with Monte Carlo calculations, for the visible and 2.2 μm spectral bands of Table 1 (columns) and three cloud optical thicknesses (rows). Results are shown as a function of solar and viewing geometry, for a cloud with an effective radius of 10 μm. Because of significant structure in the contour plots, exact reciprocity was ensured by averaging Monte Carlo calculations for reciprocal angles (transport estimates using average scattering values from superposition formulae automatically satisfy reciprocity). (b) Same as Fig. 6a but relative error in the estimated transport of transmitted photons.

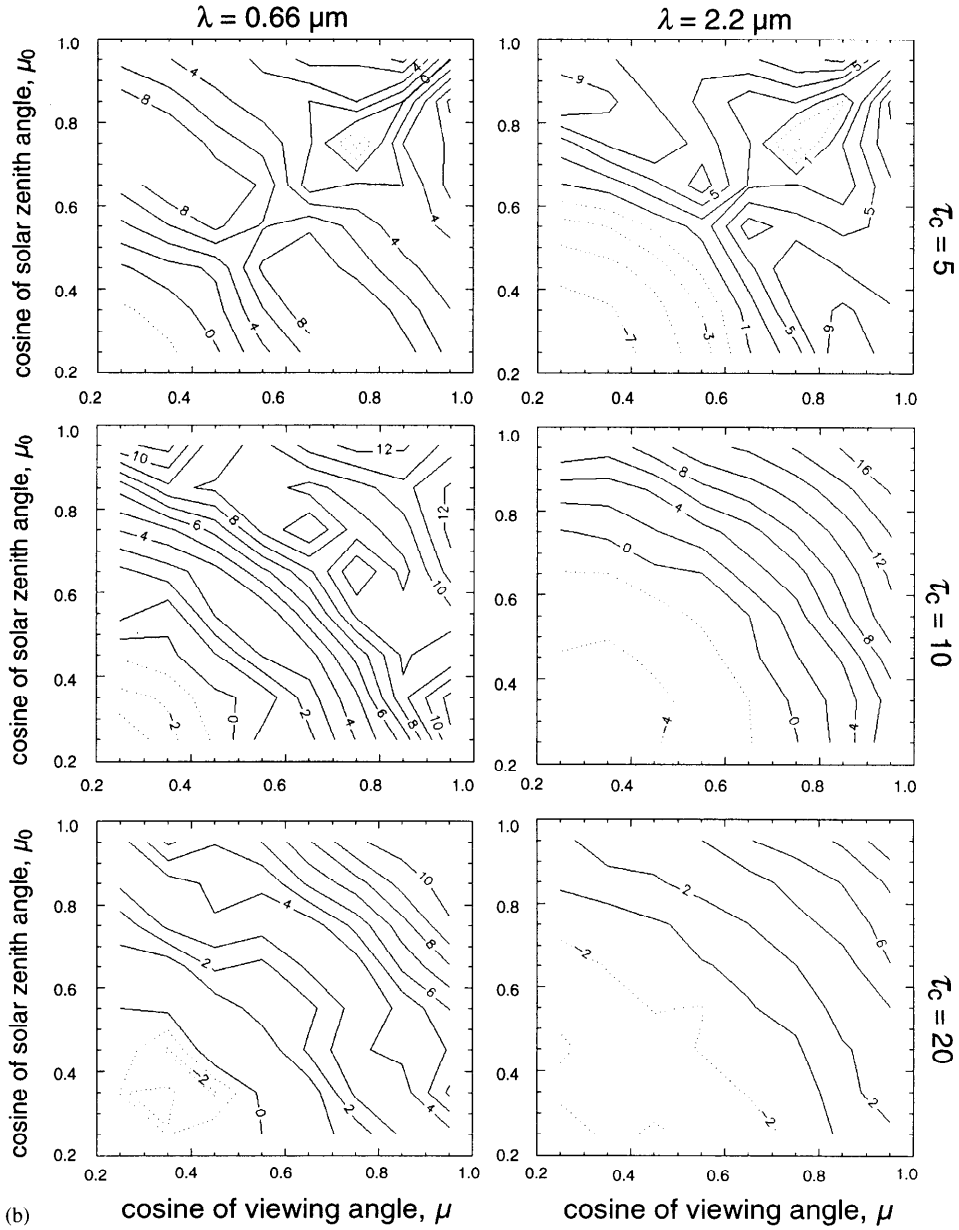

Fig. 6. (*continued*).

curvature of the log of the distribution versus optical path becomes negative (second derivative less than zero) at the shorter path lengths; conversely, curvature becomes positive in this region when $\alpha < 1, f > \sqrt{2}$. The distribution always becomes exponential at longer path lengths with larger α's resulting in greater exponential decay.

Eq. (8) was tested against horizontal transport distributions derived from Monte Carlo calculations for the spectral bands of Table 1. Comparisons are shown in Fig. 7. The analytic function is seen to provide an excellent fit in all bands for both reflectance and transmittance cases. Note that the negative curvature seen in the plots implies $\alpha > 1, f < \sqrt{2}$ (not always true, see Figs. 8 and 9).

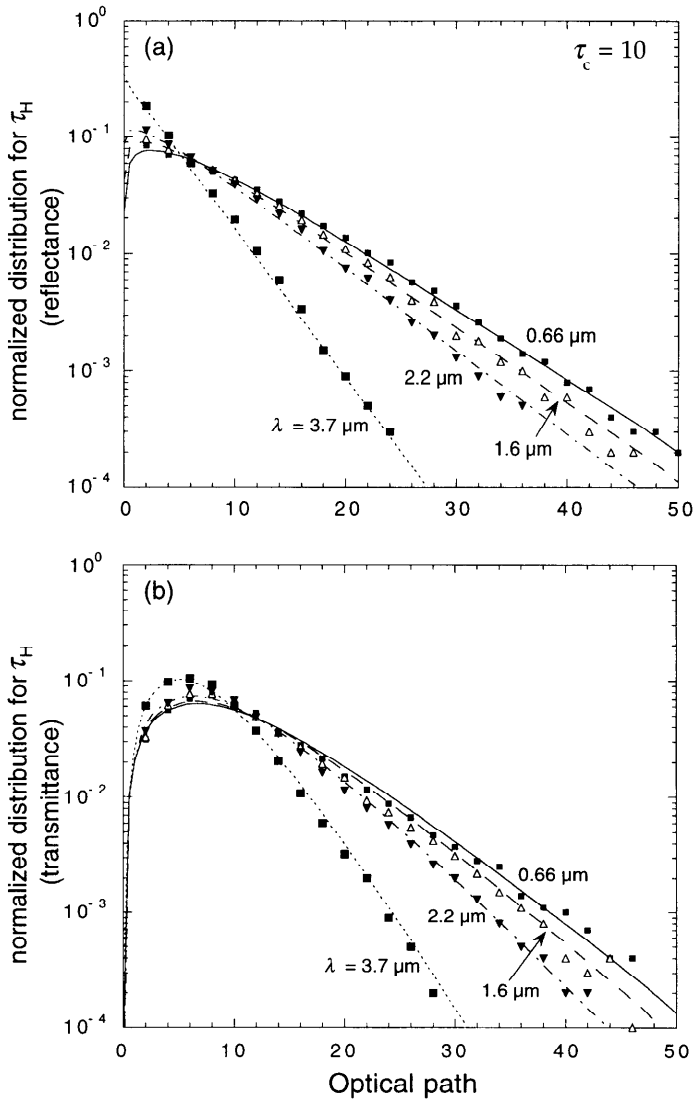

Fig. 7. Probability distribution functions for the horizontal optical path displacement of (a) reflected, and (b) transmitted photons are well approximated by the analytic gamma distribution (lines) for the visible and near-infrared bands of Table 1, as shown in this comparison with Monte Carlo calculations (symbols). Calculated for flux reflectance and transmittance, $\tau_c = 10$, $r_e = 10$ μm, and $\mu_0 = 0.65$. The two parameters needed for the gamma function, the root-mean-square and average radial displacement, are taken from the Monte Carlo calculations.

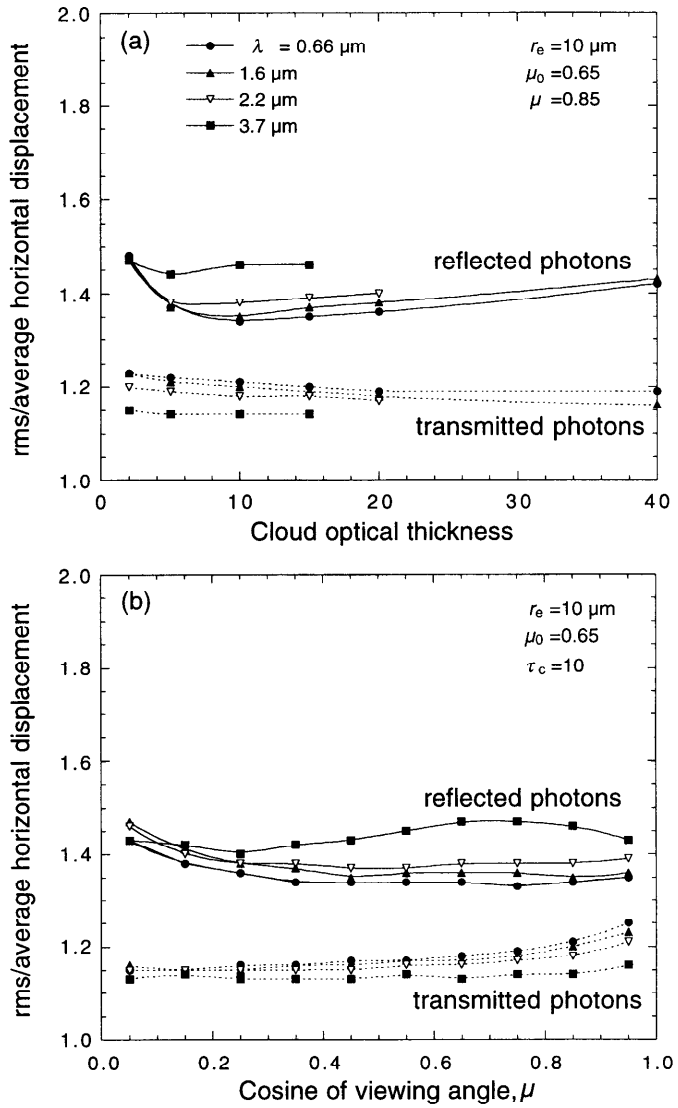

Fig. 8. The ratio of the horizontal r.m.s. photon displacement to the average radial horizontal displacement is found to be remarkably constant as a function of wavelength, cloud optical thickness and geometry, for both reflected and transmitted photons, for the cases considered. From Monte Carlo calculations with $r_e = 10$ μm.

Of the two parameters needed in Eq. (8), only $\tau_{H,r.m.s.}$ is available from the approximations of Section 2. However, Monte Carlo calculations indicate that the average displacement is related to the r.m.s. by a relatively constant factor across a broad range of optical thicknesses, solar/viewing geometries, and spectral bands. Fig. 8a gives the ratio f as a function of cloud optical thickness for selected solar and viewing angles in the four spectral bands of interest. The ratios are nearly equal with optical thickness (which spans the typical range of terrestrial values) and across all bands.

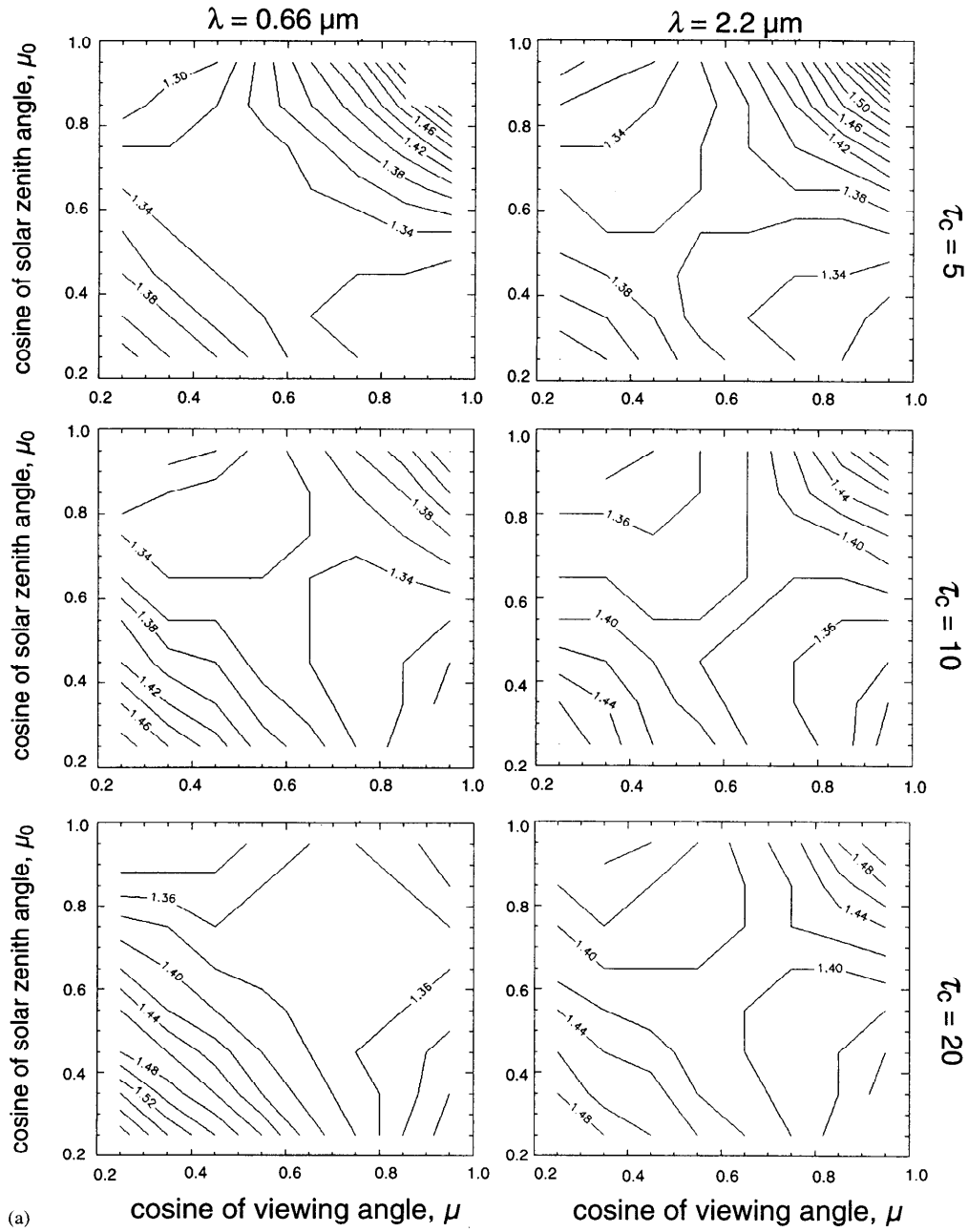

Fig. 9. (a) Monte Carlo calculations of the ratio of the r.m.s. reflected horizontal displacement to the average radial displacement for the visible and 2.2 μm band of Table 1 (columns) and three cloud optical thicknesses (rows), as a function of solar and viewing geometry, for $r_e = 10$ μm. Reciprocity holds for the two angles, though exact symmetry is limited by Monte Carlo statistical noise. (b) Same as Fig. 9a, but the ratio for transmitted photons.

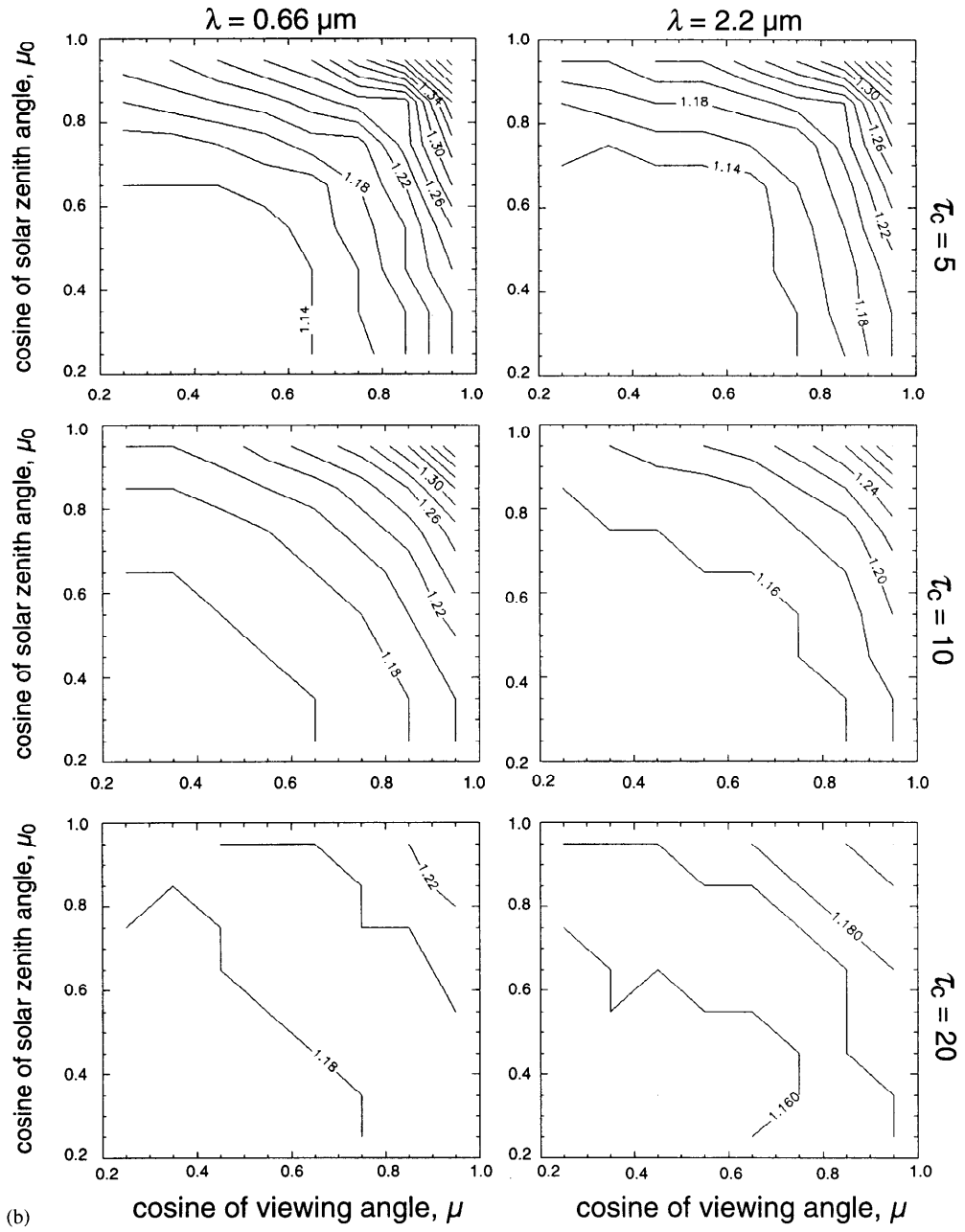

(b)

Fig. 9. (*continued*).

With the exception of the 3.7 μm band, the ratios are about 1.35–1.40 for reflectance, and somewhat smaller for transmittance at about 1.2. There is a slight increase (decrease) in the ratio with wavelength for reflectance (transmittance). However, even the 3.7 μm band ratios are acceptably

close in value to the other bands for approximation purposes. Fig. 8b gives the ratios for fixed optical thickness, $\tau_c = 10$, and solar zenith angle. Again the ratios are tightly constrained about the same values. With regard to Eq. (8), relatively constant values for the ratio f as a function of geometry and thickness correspondingly constrain values for the parameter α in the analytic distribution, leaving a single unknown parameter.

The explanation for a fixed value of f is not immediately obvious. However, Davis et al. [23] investigated similar ratios in their study of cloud lidar backscatter returns. In particular, for 2-stream reflectance from homogeneous conservative scattering clouds, they derived asymptotic formulae for the first and second moment of the total photon path length as well as the r.m.s. horizontal path displacement (referred to as "spot size"). Their calculations show that the ratios $l_{T,r.m.s.}/\langle l_T \rangle$ and $\tau_{H,r.m.s.}/\langle l_T \rangle$, where l_T is the total photon optical path length, are constant up to a scaled cloud optical thickness of about $(1-g)\tau_c \approx 2-3$. However, as thickness increases beyond this range, $l_{T,r.m.s.}/\langle l_T \rangle$ increases as $[(1-g)\tau_c]^{1/2}$, in the asymptotic limit, while $\tau_{H,r.m.s.}/\langle l_T \rangle$ decreases as $[(1-g)\tau_c]^{-1/2}$. Both quantities are closely related to f. Motivated by the asymptotic behavior of these ratios, flux reflectance and transmittance calculations (with $\mu_0 = 0.65$) were made for all relevant quantities over an extended range of optical thicknesses. At small thicknesses, f is found to be identical to $l_{T,r.m.s.}/\langle l_T \rangle$. Likewise, f eventually begins to increase with optical thickness, though more slowly, being proportional to $[(1-g)\tau_c]^{1/4}$ in the asymptotic limit. Nevertheless, f is effectively constant for terrestrial clouds as already noted. Even up to $\tau_c = 150$, f is approximately linear with optical thickness having a slope of only 0.003. Consistency with the observed asymptotic behavior of f requires $\langle \tau_{II} \rangle / \langle l_T \rangle \propto [(1-g)\tau_c]^{-3/4}$ or $\langle \tau_H \rangle \propto [(1-g)\tau_c]^{1/4}$ which is also borne out in the calculations (compare with $\tau_{H,r.m.s.}/l_{T,r.m.s.} \propto [(1-g)\tau_c]^{-1}$ from asymptotic theory). That is, as expected, average horizontal displacement quickly lags behind average total path length, though not as quickly as for the comparable r.m.s. quantities. With non-conservative scattering, both f and $l_{T,r.m.s.}/\langle l_T \rangle$ asymptotically increase to a constant value as absorption reduces long-range transport. In the case of f for example, path absorption in the 2.2 μm band limits transport before optical thickness reaches values where the ratio would otherwise begin to increase significantly, resulting in a relatively constant value at *any* optical thicknesses. For transmitted photons, both ratios remain essentially constant regardless of cloud thickness for conservative scattering; when absorption is present the ratios eventually decrease linearly with optical thickness (slope of about -0.001), though f is again more nearly constant.

The preceding results inspired a more comprehensive set of bidirectional calculations for f. Contour plots of f for reflectance transport, as a function of both solar and viewing geometry, are shown in Fig. 9a for the visible and 2.2 μm bands, and three cloud optical thicknesses ($\tau_c = 5, 10, 20$). The ratio is still relatively constant over a broad range of angles, with somewhat larger values occurring when both solar and viewing directions are towards the horizon or overhead. The departures from the nominal ratio are most dramatic for the thinner cloud ($\tau_c = 5$) where there are fewer photon scatterings. Similar contour plots are shown in Fig. 9b for transmittance. Now, above-average ratios are only found towards overhead positions, with remarkably constant values throughout the rest of the region. Again, the increase is most dramatic for the thinner cloud. The spectral results indicate that the ratio is not critically dependent on asymmetry parameter (Table 1).

In summary, calculations suggest that the average radial displacement can be reasonably well predicted from the r.m.s. value. Based on Fig. 9, r.m.s.-to-average ratios of about 1.35 and 1.18 for

reflectance and transmittance transport, respectively, appear representative for the visible. The 2.2 μm band ratios generally differ from the visible by less that 2% in a manner similar to Fig. 8, but close to 5% at overhead solar/viewing positions. The 1.6 μm band ratios will be intermediate between these two bands. Values more appropriate for particular angles and thicknesses can be obtained directly from Figs. 8 and 9. To the extent that the above results can be used to predict the ratio at other thicknesses, the two-parameter analytic form for photon transport (requiring r.m.s. and average displacements) collapses to a single parameter form (r.m.s. or average value). Therefore, in conjunction with Figs. 8 and 9, the r.m.s. horizontal displacement formulae from Section 2 can be used to estimate the full horizontal transport distribution. The accuracy in predicting the distribution obviously depends on optical thickness and solar/viewing geometry. The error calculations of Section 2.4 and Figs. 8 and 9 can be combined to estimate an overall error in approximating the distribution in this manner.

4. Conclusions

Analytic formulae for estimating the root-mean-square (r.m.s.) horizontal photon optical path transport of reflected and transmitted photons, through anisotropic, multiple scattering cloud layers, have been derived for both small and large photon scattering number regimes. Transport in the latter regime is derived from random walk theory (photon diffusion), while a modified diffusion approximation is require for the former. In both regimes, transport is expressed as a function of the average number of photon scatterings and particle single scattering parameters (asymmetry parameter and single scattering albedo). The usefulness of the transport approximation is therefore dependent on a fast and efficient means for calculating the average scattering number. It is shown in a companion paper [11] that the average number of reflected or transmitted photon scatterings occurring in an arbitrary vertically inhomogeneous, plane-parallel medium can be found accurately from superposition formulae. These formulae have been implemented with common adding/doubling numerical routines for arbitrary combinations of solar and viewing geometry. The efficiency of the superposition calculations for scattering numbers allows for the practical use of the transport approximation. Only the azimuthally averaged radiation field was considered. Approximations for 3-D transport were also discussed.

Horizontal transport estimates were compared with Monte Carlo calculations for liquid water clouds in several solar spectral bands used for cloud remote sensing, and as a function of cloud optical thickness, and solar and viewing geometry. Generally, relative error was within 10% across all these variables. The error increases for thin clouds (optical thickness less than 4), while local maxima are observed at thicknesses corresponding to the boundary between the two regimes described by Eqs. (4a) and (4b) (diffusion domain and small orders of scattering regimes, respectively).

A standard two-parameter distribution function for photon transport was shown to be applicable to horizontal transport through clouds in the spectral bands considered. The azimuthally symmetric distribution is expressed as a function of the horizontal r.m.s. and average radial displacement. Both parameters were determined from Monte Carlo calculations for a range of optical thicknesses, solar/viewing angles, and spectral bands (Figs. 8 and 9). Over most of the angular space, the ratio of the horizontal r.m.s. to the average radial displacement was found to be

tightly constrained for both reflectance and transmittance problems. These calculated ratios, in conjunction with the r.m.s. transport approximation, provide a straightforward means for estimating the full horizontal displacement distribution function.

The photon transport approximations are useful in determining the extent over which plane-parallel radiative transfer models should be realized for use with remote sensing retrievals, that is, the practical definition of the plane-parallel assumption. In a similar sense, imaging instruments collecting radiation over these scales effectively eliminates the influence of cloud regions outside the field of view.

Acknowledgements

This work was supported in part by grant NAG5-6996 from the National Aeronautics and Space Administration, EOS validation program office. The author is grateful to Dr. A. Davis for useful suggestions, and to Drs. A. Marshak and S. Twomey for many helpful discussions.

References

[1] Gerber H, Arends BG, Ackerman AS. New microphysics sensor for aircraft use. Atmos Res 1994;31:235–52.
[2] Davis A, Marshak A, Gerber H, Wiscombe W. Horizontal structure of marine boundary layer clouds from centimeter to kilometer scales. J Geophys Res 1999;104:6123–44.
[3] Cahalan RF, Snider JB. Marine stratocumulus structure. Remote Sens Environ 1989;28:95–107.
[4] Blaskovic M, Davies R, Snider JB. Diurnal variation of marine stratocumulus over San Nicolas Island during July 1987. Mon Weather Rev 1987;119:1469–78.
[5] Slingo A, Nicholls S, Schmetz J. Aircraft observations of marine stratocumulus during JASIN. Quart J Roy Meteorol Soc 1982;108:833–56.
[6] Curry JA. Interactions among turbulence, radiation, and microphysics in arctic stratus clouds. J Atmos Sci 1986;43:90–106.
[7] Loeb NG, Davies R. Angular dependence of observed reflectances: a comparison with plane parallel theory. J Geophys Res 1997;102:6865–81.
[8] Cahalan RF, Ridgway W, Wiscombe WJ, Bell TL, Snider JB. The albedo of fractal cumulus clouds. J Atmos Sci 1994;51:2434–55.
[9] Marshak A, Davis A, Wiscombe W, Cahalan RF. Radiative smoothing in fractal fields. J Geophys Res 1995;100:26247–61.
[10] Platnick S. The scales of photon transport in cloud remote sensing problems. In: Smith WL, Stamnes K, editors. IRS '96: Current Problems in Atmospheric Radiation. Hampton, Virginia: A Deepak, 1997, pp. 206–9.
[11] Platnick S. A superposition technique for deriving mean photon scattering statistics in plane-parallel cloudy atmospheres. JQSRT 2001;68:57–73.
[12] van de Hulst HC. Multiple light scattering. New York: Academic Press, 1980.
[13] Davis A, Marshak A. Lévy kinetics in slab geometry: scaling of transmission probability. In: Novak MM, Dewey TG. editors. Fractal Frontiers. Singapore: World Scientific, 1997. pp. 63–72.
[14] Bohren CF. Multiple scattering of light and some of its observable consequences. Am J Phys 1987;55:524–33.
[15] Davis A, Marshak A, Cahalan R, Wiscombe W. The Landsat scale break in stratocumulus as a three-dimensional radiative transfer effect: implications for cloud remote sensing. J Atmos Sci 1997;54:241–60.
[16] Twomey S, Jacobowitz H, Howell HG. Light scattering by cloud layers. J Atmos Sci 1967;24:109–18.
[17] Twomey S, Jacobowitz H, Howell HG. Matrix methods for multiple-scattering problems. J Atmos Sci 1966;23:101–8.

[18] Hansen JE, Travis LD. Space. Sci Rev 1974;31:527.
[19] Kaufman YJ, Herring DD, Ranson KJ, Collatz GJ. Earth observing system AM1 mission to earth. IEEE Trans Geosci Remote Sens 1998;36:1045–55.
[20] King MD, Menzel WP, Grant PS, Myers JS, Arnold GT, Platnick SE, Gumley LE, Tsay SC, Moeller CC, Fitzgerald M, Brown KS, Osterwisch FG. Airborne scanning spectrometer for remote sensing of cloud, aerosol, water vapor and surface properties. J Atmos Oceanic Technol 1996;13:777–94.
[21] Marshak A, Davis A, Cahalan RF, Wiscombe W. Nonlocal independent pixel approximation: direct and inverse problems. IEEE Trans Geosci Remote Sens 1998;36:192–205.
[22] Pfeilsticker K, Erle F, Funk O, Veitel H, Platt U. First geometrical pathlengths probability density function derivation of the skylight from spectroscopically highly resolving oxygen A-band observations: 1. Measurement technique, atmospheric observations and model calculations. J Geophys Res 1998;103:11483–504.
[23] Davis AB, Cahalan RF, Spinhirne JD, McGill MJ, Love SP. Off-beam lidar: an emerging technique in cloud remote sensing based on Green-function theory in the diffusion domain. Phys Chem Earth 1999;24:757–65.